NREL
NATIONAL RENEWABLE ENERGY LABORATORY

Novel Power Electronics Three-Dimensional Heat Exchanger

Preprint

K. Bennion, J. Cousineau, J. Lustbader, and S. Narumanchi

Presented at ITherm 2014
Orlando, Florida
May 27–30, 2014

NREL is a national laboratory of the U.S. Department of Energy
Office of Energy Efficiency & Renewable Energy
Operated by the Alliance for Sustainable Energy, LLC

This report is available at no cost from the National Renewable Energy Laboratory (NREL) at www.nrel.gov/publications.

Conference Paper
NREL/CP-5400-61041
August 2014

Contract No. DE-AC36-08GO28308

NOTICE

This report is available at no cost from the National Renewable Energy Laboratory (NREL) at www.nrel.gov/publications.

Available electronically at http://www.osti.gov/scitech

Available for a processing fee to U.S. Department of Energy and its contractors, in paper, from:

U.S. Department of Energy
Office of Scientific and Technical Information
P.O. Box 62
Oak Ridge, TN 37831-0062
phone: 865.576.8401
fax: 865.576.5728
email: mailto:reports@adonis.osti.gov

Available for sale to the public, in paper, from:

U.S. Department of Commerce
National Technical Information Service
5285 Port Royal Road
Springfield, VA 22161
phone: 800.553.6847
fax: 703.605.6900
email: orders@ntis.fedworld.gov
online ordering: http://www.ntis.gov/help/ordermethods.aspx

Cover Photos: (left to right) photo by Pat Corkery, NREL 16416, photo from SunEdison, NREL 17423, photo by Pat Corkery, NREL 16560, photo by Dennis Schroeder, NREL 17613, photo by Dean Armstrong, NREL 17436, photo by Pat Corkery, NREL 17721.

Novel Power Electronics Three-Dimensional Heat Exchanger

Kevin Bennion, Justin Cousineau, Jason Lustbader, Sreekant Narumanchi
National Renewable Energy Laboratory
1617 Cole Blvd
Golden, CO, U.S.A., 80401
Email: kevin.bennion@nrel.gov

ABSTRACT

Electric-drive systems, which include electric machines and power electronics, are a key enabling technology to meet increasing automotive fuel economy standards, improve energy security, address environmental concerns, and support economic development. Enabling cost-effective electric-drive systems requires reductions in inverter power semiconductor area, which increases challenges associated with heat removal. In this paper, we demonstrate an integrated approach to the design of thermal management systems for power semiconductors that matches the passive thermal resistance of the packaging with the active convective cooling performance of the heat exchanger. The heat exchanger concept builds on existing semiconductor thermal management improvements described in literature and patents, which include improved bonded interface materials, direct cooling of the semiconductor packages, and double-sided cooling. The key difference in the described concept is the achievement of high heat transfer performance with less aggressive cooling techniques by optimizing the passive and active heat transfer paths. An extruded aluminum design was selected because of its lower tooling cost, higher performance, and scalability in comparison to cast aluminum. Results demonstrated a 102% heat flux improvement and a package heat density improvement over 30%, which achieved the thermal performance targets.

KEY WORDS: power electronics, thermal management, electric drive, water-ethylene glycol, aluminum extrusions, electric vehicle, inverter, heat exchanger

NOMENCLATURE

A	area
Al	aluminum
AlN	aluminum nitride
CFD	computational fluid dynamics
c_p	coolant specific heat
Cu	copper
DBC	direct-bond-copper
FEA	finite element analysis
HX	heat exchanger
IGBT	insulated gate bipolar transistor
$\dot{m}$	liquid coolant mass flow
R	thermal resistance
Si	silicon
T	temperature
WEG	water-ethylene glycol

Greek symbols

ε	heat exchanger effectiveness

Subscripts

b	heat exchanger base
c	coolant
i	inlet
th,hx	heat exchanger thermal resistance

INTRODUCTION

This paper describes a heat exchanger design integrated with the power semiconductor packages to achieve high thermal performance while enabling less aggressive and potentially lower cost convective cooling technologies meeting automotive requirements. The passive and active cooling elements of the design were refined through the use of software tools for thermal finite element analysis (FEA) and computational fluid dynamics (CFD) run on a high performance computer cluster to enable batch runs over many design variables. Multiple levels of model validation were performed, including a single channel analytical model to check CFD results, full conjugate heat transfer CFD to verify FEA optimization results, and experimental validation. This work focused on application of the design to power semiconductor packages for automotive electric traction drive inverter applications.

Motivation

Electric-drive systems for vehicle propulsion enable technologies critical to meeting challenges for energy, environment, and economic security. According to the Transportation Energy Data Book, 70% of the total petroleum used in the United States is consumed by the transportation sector, which is dependent on petroleum as an energy source [1]. The President's 2013 Climate Action Plan highlights that 28% of greenhouse gas emissions were due to the transportation sector, and it emphasizes energy efficiency and technology developments to reduce emissions and increase energy security [2], [3]. Electric-drive systems, which include electric machines and power electronics, are a key enabling technology for advanced vehicle propulsion systems that reduce the dependence of the U.S. transportation sector on petroleum. To penetrate the market, however, these electric-drive technologies must enable vehicle solutions that are economically justifiable. Reducing the cost of power electronics is seen as a key enabler to electric propulsion [4].

To reduce power electronics cost, weight, and volume, the semiconductor area must be reduced. As components of the electric-drive system are made smaller, lighter, and more cost effective, heat removal becomes an increasing challenge. The vehicle must achieve the performance requirements as it operates within its thermal limitations. To successfully integrate advanced power electronics concepts into vehicle applications, the thermal limitations of the semiconductor

devices must be addressed. Increasing the semiconductor heat flux (heat per semiconductor area) reduces the required semiconductor area for the same power level. The reduced semiconductor area leads to reductions in other packaging and interconnect materials which further reduces cost, weight, and volume. This work is supported through the Department of Energy's Vehicle Technologies Office in partnership with U.S. DRIVE to reduce cost through improved thermal management [5], [6].

Current Approaches to Problem

Conventional approaches to cooling power semiconductors are limited for vehicle applications because of the thermal resistance of the passive stack of the package with typical thermal interface material (e.g. grease) between the heat spreader and the heat exchanger (see Fig. 1) [7]. Methods to improve the passive stack thermal resistance include: improving the thermal properties of thermal interfaces, eliminating thermal interfaces such as the grease layers by integrating the heat exchanger into the package (referred to as direct cooling), and employing double-sided cooling.

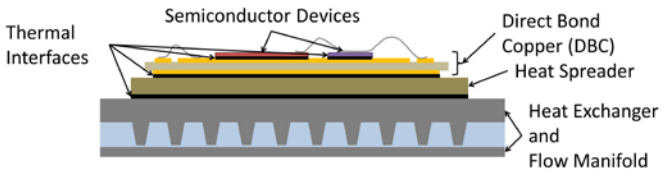

Fig. 1 Conventional power electronics semiconductor thermal stack with heat spreader and thermal interface material between the heat spreader and the heat exchanger surface.

Improvements to large area thermal interfaces can have a significant impact on improving the passive stack thermal resistance [7]. Research into developing and characterizing the performance and reliability of large area attach methods is critical in reducing the passive stack thermal resistance [8], [9]. The cooling approach described in this paper benefits from interface material research, and future work could utilize improvements in large area bonding methods.

Double-sided cooling improves the power per die area of power semiconductors by increasing the available area for heat transfer. The benefits of double-sided cooling and example implementations are summarized in the following sources [10]–[18]. Double-sided cooling requires a passive stack cooling structure and electronics packaging capable of cooling both sides of the semiconductor package. This work attempts to develop a cooling approach that is compatible with single-sided and double-sided cooling.

Another approach to improving the power capability of power semiconductor devices is direct cooling. Through direct cooling, elements within the package with higher thermal resistance are removed from the heat transfer path by removing layers and applying the convective cooling closer to the heat source. The benefits of direct cooling as highlighted by Skuriat and Johnson [19] include reduction of package thermal resistance through removal of material layers such as grease, and conventional cold plates. Also, Skuriat and Johnson mention fewer interfaces with different thermal expansion coefficients lead to potential improvements in thermal reliability.

Multiple methods have been used or proposed for direct cooling of the semiconductor. One approach involves removing the grease thermal interface material and directly cooling the base plate or heat spreader of the power semiconductor module. Examples include pins molded or machined into the heat spreader [20]–[22], folded fins bonded to the heat spreader [23], or jet impingement onto the heat spreader [24]–[26]. Beside cooling the base plate, other examples include directly cooling the substrate material or the metalization layers on the substrate, such as direct bond copper (DBC), using jets [27]–[30], or through the use of microchannels [31], [32]. Also, microchannels within the silicon and silicon carbide layers have been investigated [33]–[35]

As layers are removed within the package to reduce the passive stack thermal resistance, typically the available footprint area to which cooling can be applied is also reduced. The reduction in area necessitates higher performing or more aggressive cooling technologies. For this reason, the cooling performance must be matched to the package design to get the optimal integrated solution [10], [36]. The more aggressive cooling can potentially be difficult to manufacture in high-volume applications required for automotive systems, which shifts more cost into the thermal management system. The increased cost can reduce or cancel the cost savings of reduced silicon area.

When developing a package that is directly cooled, other thermal bottlenecks could be introduced in the power electronics system that might reduce the effectiveness of the proposed thermal design. Possible examples include the following items. The thermal performance of the power semiconductor could degrade by increasing the thickness of low thermal conductivity materials. An integrated package requires methods of bonding or attaching the cooling interface to the package that are capable of withstanding the potential thermal stresses. The bonded interface can lead to thermal bottlenecks. Unlike applications that have steady continuous loads, electric-drive systems in vehicle applications experience significant dynamic changes in loading. The effective thermal capacitance of the packaging structure provides some support in reducing the magnitude of temperature cycles [37], [38] and the impact on reliability. Also, improvements in semiconductor thermal management often focus on the semiconductor and neglect other temperature sensitive power electronics components. For example, the bus bars can conduct heat to other components [39]. Finally, another concern is related to sealing of the cooling system to prevent coolant leaks into the electronics [21].

APPROACH

We optimized the passive and active thermal design components for an inverter application. The passive thermal design focused on the mechanical structure of the semiconductor package and heat exchanger. The thermal performance of the passive components is a function of the layer material properties, interfaces, and the layer material geometries. The passive thermal performance is also affected

by the technology selected for the active thermal design. The active thermal design focused on the convective cooling interface between the heat exchanger and the cooling fluid. A cost effective solution requires matching the passive thermal design with the active cooling design. The approach to designing an integrated passive and active thermal management system for power semiconductor modules included developing design specifications, designing the prototype, and testing the concept experimentally.

Design Specifications

The design specifications emphasize thermal management because the project focused on thermal management of the power semiconductor devices and not development of a full inverter. The achievable power per silicon area directly impacts the cost of power electronics, which is limited by the ability to remove heat. For this reason, the heat removed from the Insulated Gate Bipolar Transistor (IGBT) per footprint area of the IGBT was the primary metric to illustrate the potential relative cost benefit. The design target was to double the IGBT heat flux as compared to a best-in-class commercial module.

A cost effective thermal management approach also required compatibility with established high volume manufacturing methods used within automotive applications. Examples include aluminum castings, brazed fins, and aluminum extrusions. The selected design focused on using aluminum extrusion techniques to reduce fabrication cost through adherence to industry supplied guidelines and reducing voids or hollow channels within the part. The design also emphasized a modular, scalable, and flexible design. A modular design allows the package to be reused and has broader applications. For example, the goal was to develop a thermal design that could scale up in power requirements without the need for a complete redesign of a heat exchanger casting. Another reason an aluminum extrusion process was selected is because aluminum extrusions can have higher thermal conductivity and lower cost as compared to cast structures if designed properly for the targeted application.

In addition to cost, the volume of the power electronics is another critical design goal because of space limitations within a vehicle. The volume of the power electronics not only depends on the size of the components but also on how densely the components can be packaged while still removing heat. The volume specifications were described in terms of the power module heat density. The power module heat density is defined as the total heat removed divided by the total volume of the semiconductor power module packaging and heat exchangers. The design target was to maintain or exceed power module heat density as compared to a best-in-class commercial module.

Additional design constraints focused on factors to reduce failure modes associated with the thermal management system. The minimum coolant channel dimensions must allow a 1 mm particle to pass through the cooling system without clogging. Eliminating internal fluid seals around the power semiconductor devices reduces the impact of fluid leaks within the electronics. Maintaining or increasing thermal capacitance of the module reduces the sensitivity to temperature cycling. Finally, the design should also be compatible with cooling or isolating other temperature sensitive components within the power electronics. For example, bus bar cooling could thermally isolate temperature sensitive components and suppress heat transfer from the motor to the inverter [39].

To consistently evaluate progress towards the design specifications, the following analysis assumptions were applied. The IGBT and diode operating losses or heat loads were proportioned with an IGBT-to-diode heating ratio of three to one. The maximum semiconductor (IGBT, diode) temperature was limited to 150°C to calculate the maximum heat flux removal rates. Liquid cooling with a 50/50 by mass mixture of water-ethylene glycol (WEG) was assumed. The design flow rate at the inverter system level was 1.67e-4 m^3/s (10 L/min) with a 70°C inlet coolant temperature.

The package structure was limited to conventional in-use materials as shown in Fig. 2. However, removal of layers was allowed. The design was also required to be compatible with single-sided and double-sided cooling. Focusing on existing packaging methods and materials prevented the introduction of unknown costs through new materials or manufacturing processes. The material properties are listed in Table 1.

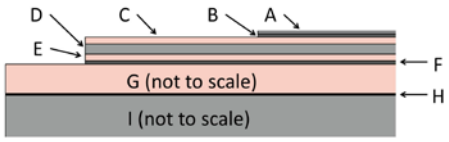

Fig. 2 Schematic of package layers.

Table 1. Material properties included in analysis

Layer		Material	Thermal Conductivity [W/m-K]
A	IGBT/Diode	Si	92
B	Bonded Interface	Solder	51
C	Metalization	Cu	394
D	Substrate	AlN	140
E	Metalization	Cu	394
F	Bonded Interface	Solder	51
G	Heat Spreader	Cu or Aluminum (Al) 6063	394 or 210
H	Thermal Interface	Grease	1.5
I	Heat Sink	Al 6061	154

Design Approach

We identified the appropriate passive and active thermal designs to meet performance targets through comparison to selected baseline packages. We optimized the selected passive thermal design and identified the active thermal design targets. The primary commercial system benchmark was the power module used within the LS 600h hybrid system, which is described in detail in [11], and the thermal performance is based on analysis described in [10]. The LS 600h package was selected because of its best-in-class performance as benchmarked through the Vehicle Technology Office Advanced Power Electronics and Electric Motors activity. The design is also similar to recent hybrid systems for lower cost vehicles. Potential designs were also compared against direct

cooling approaches for a direct-cooled base plate and direct-cooled DBC. The direct-cooled DBC performs best at low thermal resistance as seen in Fig. 3.

The targeted minimum heat exchanger cooling resistance was between 100 to 200 mm^2-K/W, shown in Fig 3. This range represents typical channel flow cooling with WEG. The ability to enable higher resistance, leads to potential cost reductions in the heat exchanger fabrication and increased system robustness. Fig. 3 highlights that the existing direct cooling approaches do not achieve the desired IGBT heat flux improvement within the targeted active cooling performance region. The targeted active cooling performance region in Fig. 3 is defined as the heat exchanger thermal resistance defined below in Equation 1. The heat exchanger thermal resistance ($R_{th,hx}$) is based on the cooled base area (A_b), heat exchanger effectiveness (ε), coolant mass flow ($\dot{m}$), and coolant specific heat (c_p) [40].

$$R_{th,hx} = {A_b}/{\varepsilon \dot{m} c_p} \quad (1)$$

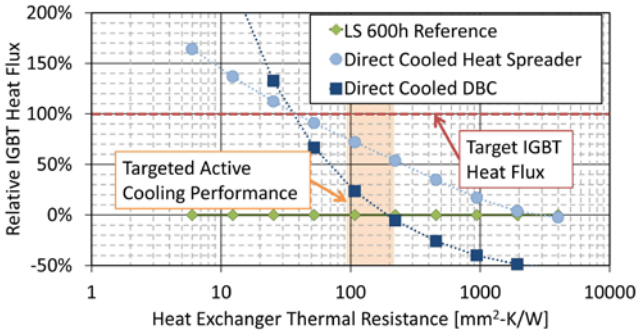

Fig. 3 Package comparison against targets assuming ability for double-sided cooling on all configurations.

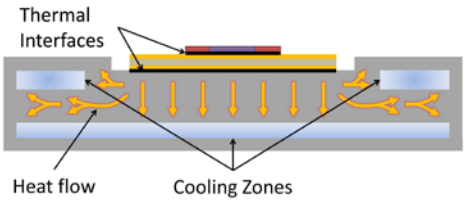

Fig. 4 Conceptual drawings of integrated heat spreader and heat exchanger system to enhance heat spreading and cooling performance.

After establishing the active cooling target, the task of designing a passive thermal system was initiated to meet the performance targets. The heat spreader geometry was optimized in FEA for the targeted active cooling convection coefficient range. The final passive cooling design is illustrated in Fig. 4. The design removes the heat sink and grease thermal interface layers (layers "H" and "I" in Fig. 2) to directly cool the heat spreader. The expanded heat spreader increases the cooled area by cooling both the back side of the heat spreader and the exposed package side of the heat spreader. Unlike conventional cooling approaches that are dominated by one dimensional heat transfer to a heat exchanger, the design enables heat to spread in all directions to multiple cooling zones within the heat spreader. For this reason it is described as a three-dimensional heat exchanger. The design process required an iterative procedure to meet the IGBT heat flux and module heat density targets within the minimum active cooling performance target. For each design, the volumetric IGBT and diode heat loads were adjusted until the maximum IGBT temperature limit of 150°C was reached. Efforts were made to maintain simple geometries to enable the use of aluminum extrusions based on industry input, and the general concept was described in a patent [41].

Once the passive thermal stack was designed, the next step involved designing the active cooling surface through both FEA and CFD analysis. CFD modeling tools enabled the evaluation of multiple cooling channel geometries. Throughout the analysis the models were checked for mesh independence and conservation of mass and energy. In the absence of preexisting experimental data for the preliminary design, other methods of cross checking the model accuracy were employed. The channel convection coefficients were compared against analytical estimates, while model decomposition of full conjugate heat transfer CFD simulations provided preliminary tests for modeling errors. The full conjugate heat transfer CFD conduction and convection results were checked independently. Separating the conduction and convection results provided comparisons to simplified models with boundary conditions calculated from the full conjugate heat transfer CFD simulations. Mapping the convection coefficient obtained from the CFD simulation to an FEA model enabled comparison of the solid-only heat conduction model accuracy of the CFD simulation.

The final design was developed with an emphasis on ease of manufacture based on industry input to enable less aggressive cooling while achieving the thermal performance targets. A few of the key design features relevant to the aluminum extrusion process are highlighted in Fig. 5. The coolant channels and fins were made as large as possible to reduce channel clogging concerns and to increase ease of extrusion. The open "E-fin" shape within the connected channels significantly reduces the cost of the extrusion by reducing the number of internal voids and the extrusion complexity. The rounded corners and minimum wall thickness follow recommended design guidelines for aluminum extrusions based on input from Sapa Extrusions North America. The final prototype design is shown in Fig. 6 with flanges on the inlet and outlet for attachment to the experimental test setup. A heater is also shown in the figure mounted to the heat exchanger for thermal testing.

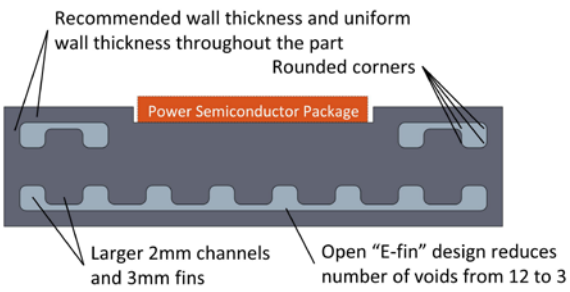

Fig. 5 Sample parameters from design guidelines to reduce fabrication cost.

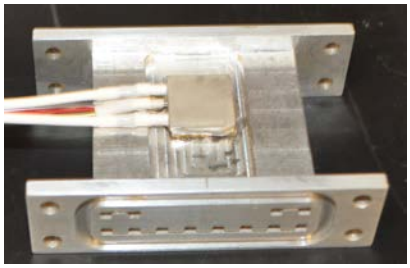

Fig. 6 Prototype design with flanges for connection to experimental test setup and a heater for thermal testing.

Experimental Approach

Once the design was selected, three heat exchangers were built. Two heat exchangers representing the design were built with Al alloy 6061 and Al 6063. The third heat exchanger, representing a baseline with a single cooling zone beneath the package, was made with Al 6061. The baseline and design heat exchanger geometries are shown in Fig. 7. The intended target material was Al 6063 because it is commonly used in extruded shapes, and it has a higher thermal conductivity relative to Al 6061. Al 6061 was used initially to build two heat exchangers for comparing the design against the baseline geometry and validate CFD modeling. Al 6061 was selected for the initial tests because of availability of the bulk material. Later a third prototype was manufactured using Al 6063 provided by Sapa Extrusions North America, which was used to confirm the expected performance benefit over Al 6061. The fabricated heat exchangers and materials are summarized in Table 2.

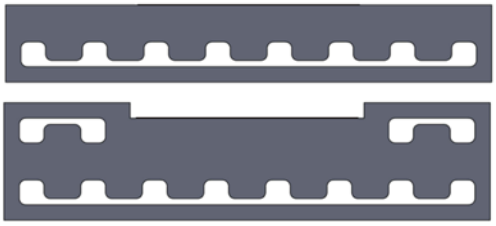

Fig. 7 Fabricated heat exchanger geometries showing baseline (top) and design (bottom).

Table 2. Tested heat exchangers and materials

Geometry	Material
Baseline	Al 6061
Design	Al 6061
Design	Al 6063

To test the prototype heat exchangers and validate the modeling results, we designed and built the experimental apparatus highlighted in Fig. 8. The prototype heat exchanger was installed between two manifolds of similar design. The coolant flow develops in the manifold prior to entering the heat exchanger channels to isolate potential flow variations caused by the inlet and outlet connections to the fluid test bench. The manifolds also provide locations for measuring inlet and outlet temperatures and pressures. The manifolds were designed using CFD models to determine the temperature and pressure measurement locations. The pressure taps are located upstream of the temperature measurements.

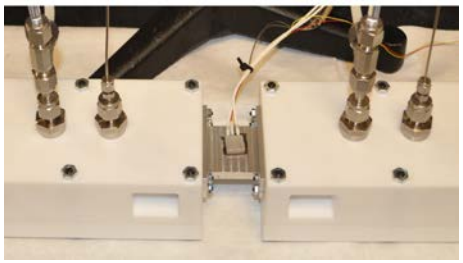

Fig. 8 Heat exchanger installed in test fixture with inlet and outlet temperature and pressure measurements.

As shown in Fig. 6, a ceramic heater was used to simulate a power semiconductor device heat load. The heater was mounted to a copper spreader with epoxy (Fig. 9). The copper spreader was bonded to the heat exchanger with a thermoplastic material made by Btechcorp (referred to in this paper as Btech). The copper spreader was instrumented with thermocouples in two locations (Fig. 10). The thermocouples were soldered into machined grooves in the copper spreader to ensure good thermal contact. To prevent damage to the heating element, the heater also included a temperature measurement.

The measurement uncertainties of temperature and pressure were estimated according to the 95% uncertainty model (U_{95}) [42], including both systematic and random errors. The type K thermocouples were calibrated over the operating temperature range using a reference (NIST traceable) probe and calibration bath. The total U_{95} confidence interval for the temperature measurements were within ±0.13°C (~0.4% of average measurement). The inlet and outlet pressures were monitored with a U-tube manometer with a U95 of ±14 Pa (~1% of average measurement).

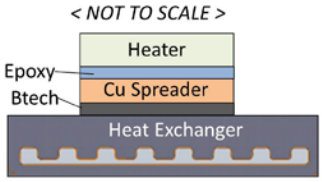

Fig. 9 Heater assembly layers and attachment to heat exchanger.

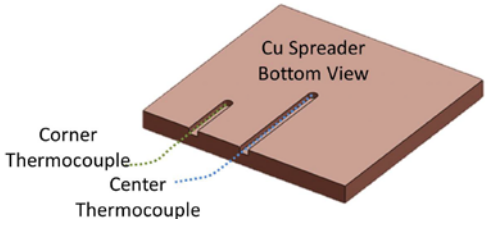

Fig. 10 Thermocouple locations in the copper spreader.

Each of the heat exchangers listed in Table 2 was tested experimentally to verify the simulated thermal and fluid characteristics of the heat exchanger from the CFD simulation results. The model validation experiments were performed with a WEG mixture of 50%/50% by volume. The heat exchangers were tested at 0.033 kg/s, 0.067 kg/s, and 0.1 kg/s (1.9 L/min, 3.8 L/min, and 5.7 L/min). The tests for each heat exchanger included six repetitions for each test condition. Due to equipment limitations and safety, the inlet coolant temperature was set to 30°C for each test. The Specific gravity of the WEG was checked prior to starting tests to ensure the fluid properties remained consistent and similar to the simulated coolant properties.

The epoxy layer and the Btech layer illustrated in Fig. 11 represented unknown thermal resistance within the passive thermal stack. The values for these thermal resistances were estimated by matching the temperature measurements at the lowest flow rate to the model results at the same fluid flow rate and fluid properties. The process for determining the effective thermal conductivity of the epoxy and Btech layers followed the steps listed below.

1. The convection coefficients were mapped from a single flow rate CFD model to the channels in the FEA model.
2. The effective thermal conductivity of the epoxy and Btech layers were solved iteratively for a single test by matching the temperature change between the heater to copper spreader and the temperature change between the copper spreader to the inlet coolant temperature (Fig. 11).
3. The effective thermal resistance values for the epoxy and Btech layers were applied to the CFD model and validated against experimental results for other flow rates.

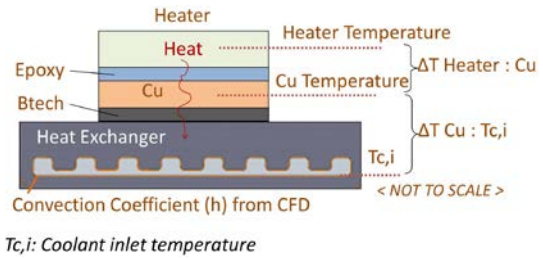

Fig. 11 Interface thermal resistance estimation for epoxy and Btech bonding layers.

Using the above approach for each of the prototype heat exchangers, we validated the CFD model results against the experimental data. The corner thermocouple temperature measurement in the copper spreader was compared against a corresponding point within the CFD model. Fig. 12 compares the difference between the experimental temperature and CFD model temperature within the copper spreader block. The magnitude of the difference between the model and the experimental results was found to be within about 2% over all of the flow rates and heat exchangers tested. This accuracy was within the targeted magnitude limit of 10%.

Fig. 13 compares the experimentally measured pressure drop with the CFD model results. The magnitude of the difference between the model and the experimental results was within about 9% across all flow rates and heat exchangers that were tested. With the analysis, it was found that the pressure drop was affected by small variations in the channel geometry. We used a high-resolution digital microscope to measure the manufactured channel dimensions for each heat exchanger and applied the averaged results to the CFD model geometries corresponding to each heat exchanger. This substantially improved the agreement of the CFD simulation results with the experimental results for all flow rates. The difference between the model and experimental results was within the targeted maximum magnitude of 10%.

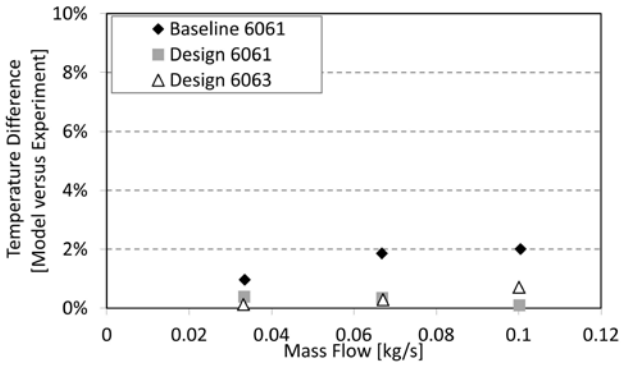

Fig. 12 Temperature validation for all tested heat exchangers across all flow rates.

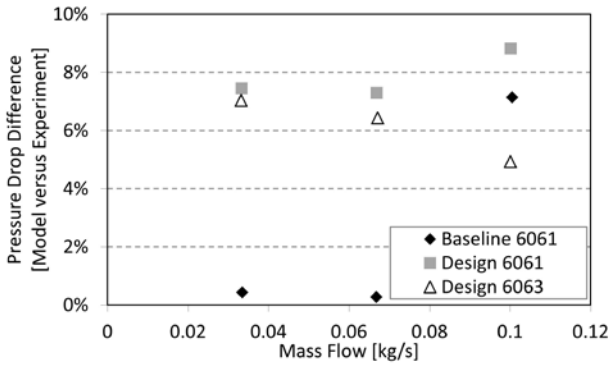

Fig. 13 Pressure validation for all tested heat exchangers across all flow rates.

RESULTS

The design met or exceeded the thermal system level (heat exchanger and semiconductor package) performance targets within the established design constraints and evaluation criteria. The combined semiconductor package model and validated heat exchanger model confirmed the expected system level performance impacts. The system level impacts of the heat exchanger design were determined through simulation using the validated heat exchanger CFD model. The system performance as compared to the baseline reference package is shown in Fig. 14. The primary goal of the research was to enable high thermal performance (IGBT heat flux) with less aggressive cooling (higher heat exchanger side thermal

resistance). Early in the design process, a targeted cooling performance range was identified as highlighted in Figs. 3 and 14, which was selected from past experience related to power electronics cooling with WEG. As seen in Fig. 14, the final design achieves the targeted improvement of a 100% improvement in IGBT heat flux within the targeted cooling performance region.

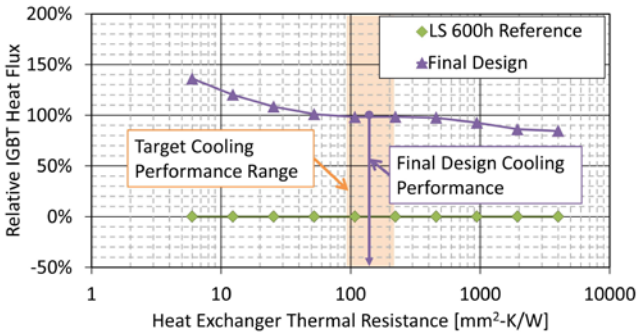

Fig. 14 Thermal FEA comparing IGBT heat flux of heat spreader design showing the original target cooling performance range and the final design.

Fig. 15 compares the design against the LS 600h reference package and the baseline aluminum heat exchanger described in Fig. 7. The comparison in Fig. 15 is at the equivalent flow rate for the LS 600h package (0.0086 kg/s per side of package), which is based on referenced modeling and analysis efforts [10]. At an equivalent flow rate, the design improves the IGBT heat flux by a factor of 1.6 with a slight improvement in package heat density. When the flow rate is held constant, the pressure drop across the design heat exchanger is significantly lower than the LS 600h reference. With the improved heat transfer and reduced pressure drop, the coefficient of performance for the design improves by a factor of 7.9 as compared to the reference LS 600h package.

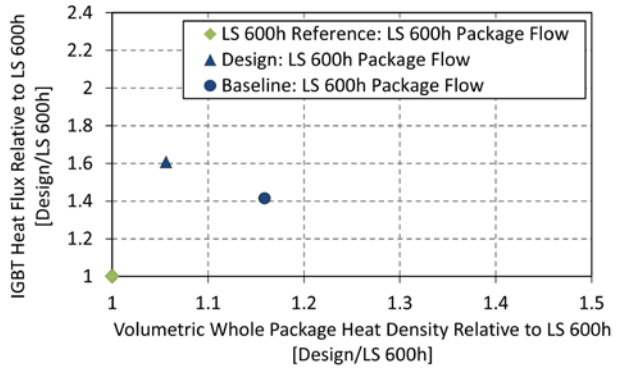

Fig. 15 Model results for design and baseline comparison at LS 600h package flow rate.

When evaluated at the target system flow rate of 1.67e-4 m^3/s (10 L/min) in the parallel configuration shown in Fig. 16, the design meets the performance targets defined at the beginning of the work. Fig. 16 shows the results with 1/6 of the system coolant flowing into each package. The IGBT heat flux improved by 102% and the package heat density improved by 32%. The design heat exchanger also exceeds the performance of the baseline at the same fluid parasitic power.

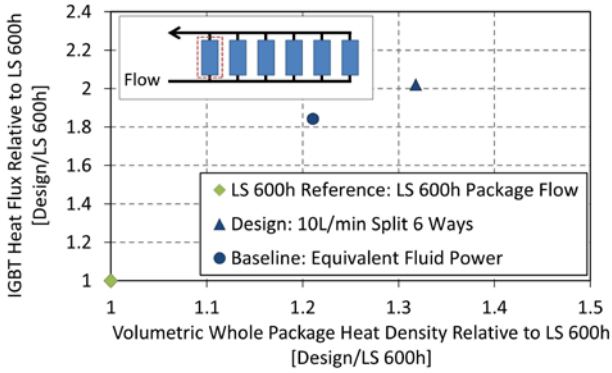

Fig. 16 Model results for design at target flow and baseline at equivalent parasitic fluid power.

As mentioned previously, the design was based on a parallel arrangement of the heat exchangers as shown in Fig. 16 with one package or module per cooling branch. Preliminary investigations were also performed to investigate the impact of series connections on the effective convection coefficient within the channels. Fig. 17 compares the average convection coefficient within the channels for three separate heat exchangers connected in series. As seen in Fig. 17, the convection coefficient drops as the flow passes through the first heat exchanger. The convection coefficient appears to stabilize as the flow passes through the second and third heat exchangers. The drop in the convection coefficient would need to be investigated as part of future work depending on the intended application. We attributed the drop in convection coefficient to the flow becoming fully developed by the time it reaches the second heat exchanger.

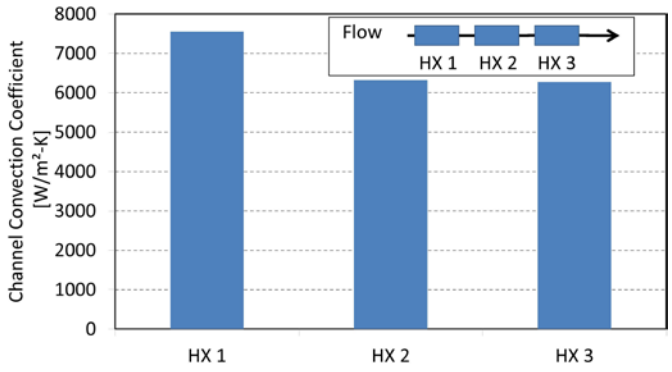

Fig. 17 Effective channel convection coefficient in each section.

SUMMARY AND CONCLUSIONS

This work focused on the development and demonstration of a concept to enable less aggressive cooling while improving the system-level semiconductor package thermal performance to improve the capability of power semiconductor devices.

The improved power capability directly relates to improving the cost per power of the power electronics. The performance of the design was compared against two baseline packages of power semiconductor devices. The design doubled the IGBT heat flux capability relative to the LS 600h reference with significant improvements in the coefficient of performance. The LS 600h package was selected as the reference because of its best-in-class performance of the modules benchmarked through the Vehicle Technology Office's Advanced Power Electronics and Electric Motors activity. The design also outperformed the baseline direct-cooled base plate configuration with similar extruded fin geometry.

The design approach built upon a recently issued patent [41] to enable high performance with less aggressive cooling. Future work could extend the concept to enable other cooling technologies with less effective coolants such as air or automatic transmission fluid. Directly cooling the power electronics with air or automatic transmission fluid could eliminate the dedicated WEG loop for cooling the power electronics and lead to potential cost reductions and elimination of cooling system components. While the design included efforts to enable cooling of bus bars or other temperature sensitive components, additional design analysis and refinements are needed in these areas specific to target applications. Also, research into improved large area bonding materials with good thermal performance and temperature cycling ability is necessary. The current work assumed a bonded interface between the DBC and heat spreader with equivalent thermal performance as solder. Additional work is needed to evaluate the reliability of high thermal performance bonded interfaces between the DBC and aluminum heat spreader used in this proposed design.

This work developed an integrated design process and applied the process to design an integrated power module heat exchanger, which builds on existing developments in bonded interfaces, direct cooling, and double sided cooling. The specific design can go through additional refinement for specific power electronics applications and this work will be included in future industry collaborations related to cooling power electronics.

ACKNOWLEDGMENTS

The authors would like to acknowledge the support provided by Susan Rogers and Steven Boyd, Technology Development Managers for Advanced Power Electronics and Electric Motors, Vehicle Technologies Office, U.S. Department of Energy Office of Energy Efficiency and Renewable Energy. The significant contributions of Sapa Extrusions North America to the project are acknowledged.

REFERENCES

[1] S. Davis, S. Diegel, and R. Boundy, *Transportation Energy Data Book*, 32nd ed. Oak Ridge National Laboratory, 2013.

[2] "The President's Climate Action Plan," Jun-2013. [Online]. Available: http://www.whitehouse.gov/sites/default/files/image/president27sclimateactionplan.pdf. [Accessed: 21-Aug-2013].

[3] The White House, "President Obama's Plan to Fight Climate Change," 25-Jun-2013. [Online]. Available: http://www.whitehouse.gov/share/climate-action-plan. [Accessed: 21-Aug-2013].

[4] "EV Everywhere Grand Challenge Blueprint." [Online]. Available: http://www1.eere.energy.gov/vehiclesandfuels/electric_vehicles/pdfs/eveverywhere_blueprint.pdf. [Accessed: 08-Aug-2013].

[5] "Vehicle Technologies Office: Advanced Power Electronics and Electrical Machines." [Online]. Available: http://www1.eere.energy.gov/vehiclesandfuels/technologies/electronics/index.html. [Accessed: 10-Sep-2013].

[6] U.S. Drive, "Electrical and Electronics Technical Team Roadmap," *Partnership Plan, Roadmaps, and Other Documents*, Jun-2013. [Online]. Available: http://www1.eere.energy.gov/vehiclesandfuels/pdfs/program/eett_roadmap_june2013.pdf. [Accessed: 10-Sep-2013].

[7] S. Narumanchi, M. Mihalic, K. Kelly, and G. Eesley, "Thermal Interface Materials for Power Electronics Applications," in *11th Intersociety Conference on Thermal and Thermomechanical Phenomena in Electronic Systems (ITherm)*, Orlando, FL, 2008, pp. 395–404.

[8] D. DeVoto, P. Paret, S. Narumanchi, and M. Mihalic, "Reliability of Bonded Interfaces for Automotive Power Electronics," in *ASME 2013 International Technical Conference and Exhibition on Packaging and Integration of Electronic and Photonic Microsystems*, Burlingame, CA, 2013.

[9] T. G. Lei, J. N. Calata, G.-Q. Lu, X. Chen, and S. Luo, "Low-Temperature Sintering of Nanoscale Silver Paste for Attaching Large-Area Chips," *IEEE Trans. Compon. Packag. Technol.*, vol. 33, no. 1, pp. 98–104, 2010.

[10] K. Bennion and K. Kelly, "Rapid Modeling of Power Electronics Thermal Management Technologies," in *IEEE Vehicle Power and Propulsion Conference (VPPC)*, Dearborn, MI, 2009, pp. 622–629.

[11] T. Burress, C. Coomer, S. Campbell, A. Wereszczak, J. Cunningham, L. Marlino, L. Seiber, and H.-T. Lin, "Evaluation of the 2008 Lexus LS 600H Hybrid Synergy Drive System." Oak Ridge National Laboratory. ORNL/TM-2008/185, Jan-2009.

[12] H. Yasui, H. Ishiyama, M. Inagaki, K. Mamitsu, and T. Kikuchi, "Power Control Unit for High Power Hybrid System," presented at the 23rd International Electric Vehicle Symposium, Anaheim, California, 2007.

[13] Y. Sakai, H. Ishiyama, and T. Kikuchi, "Power Control Unit for High Power Hybrid System," SAE International, Warrendale, PA, 2007-01-0271, Apr. 2007.

[14] M. Inagaki and M. Shirai, "Stacked Type Cooler," U.S. Patent 7571759,11-Aug-2009.

[15] D. Harada and H. Ishiyama, "Power Converter and Semiconductor Device Mounting Structure," U.S. Patent Application 2006/0284308 A1.

[16] R. S. Taylor, M. A. Jeter, E. W. Gerbsch, and J. J. Ronning, "Electronics Assembly Having Multiple Side Cooling and Method," U.S. Patent 7295433,13-Nov-2007.
[17] M. Inagaki, "Easily Assembled Cooler," U.S. Patent 8151868,10-Apr-2012.
[18] M. O'Keefe and K. Bennion, "A Comparison of Hybrid Electric Vehicle Power Electronics Cooling Options," in *IEEE Vehicle Power and Propulsion Conference (VPPC)*, Arlington, TX, 2007, pp. 116–123.
[19] R. Skuriat and C. M. Johnson, "Direct Substrate Cooling of Power Electronics," in *2008 5th International Conference on Integrated Power Systems (CIPS)*, Nuremberg, Germany, 2008, pp. 1–5.
[20] F. Nishikimi and K. Nakatsu, "Power Inverter," U.S. Patent Application 2012/0170217 A1.
[21] T. Kurosu, K. Sasaki, A. Nishihara, and K. Horiuchi, "Packaging Technologies of Direct-Cooled Power Module," in *International Power Electronics Conference (IPEC)*, Sapporo, Japan, 2010, pp. 2115–2119.
[22] R. Bayerer, "Advanced Packaging Yields Higher Performance and Reliability in Power Electronics," *Microelectron. Reliab.*, vol. 50, pp. 1715–1719, 2010.
[23] T. Matsuo, H. Hamada, A. Nishihara, and M. Musou, "Power Inverter," U.S. Patent 8072760,06-Dec-2011.
[24] E. M. Dede, "Jet Impingement Heat Exchanger Apparatuses and Power Electronics Modules," U.S. Patent 8199505,12-Jun-2012.
[25] E. M. Dede, "Experimental Investigation of the Thermal Performance of a Manifold Hierarchical Microchannel Cold Plate," in *ASME 2011 Pacific Rim Technical Conference and Exhibition on Packaging and Integration of Electronic and Photonic Systems (InterPACK)*, Portland, OR, 2011, vol. 2, pp. 59–67.
[26] S. Narumanchi, M. Mihalic, G. Moreno, and K. Bennion, "Design of Light-Weight, Single-Phase Liquid-Cooled Heat Exchanger for Automotive Power Electronics," in *13th IEEE Intersociety Conference on Thermal and Thermomechanical Phenomena in Electronic Systems (ITherm)*, San Diego, CA, 2012, pp. 693 –699.
[27] G. Moreno, S. Narumanchi, T. Venson, and K. Bennion, "Microstructured Surfaces for Single-Phase Jet Impingement Heat Transfer Enhancement," *J. Therm. Sci. Eng. Appl.*, vol. 5, no. 3, Jun. 2013.
[28] V. Hassani, A. Vlahinos, and D. Bharathan, "Low Thermal Resistance Power Module Assembly," U.S. Patent 7190581,13-Mar-2007.
[29] K. Le, T. G. Ward, B. S. Mann, E. P. Yankoski, and G. S. Smith, "Power Electronics Substrate for Direct Substrate Cooling," U.S. Patent 8169779,01-May-2012.
[30] E. M. Dede, J. Lee, Y. Liu, B. Robert, and S. H. Yonak, "Computational Methods for the Optimization and Design of Electromechanical Vehicle Systems," *Int. J. Veh. Des.*, vol. 58, no. 2–4, pp. 159–180, 2012.
[31] J. Schulz-Harder, "Efficient Cooling of Power Electronics," in *3rd International Conference on Power Electronics Systems and Applications (PESA)*, Hong Kong, China, 2009, pp. 1–4.
[32] D. J. Sharar, N. R. Jankowski, and B. Morgan, "Thermal Performance of a Direct-Bond-Copper Aluminum Nitride Manifold-Microchannel Cooler," in *26th Annual IEEE Semiconductor Thermal Measurement and Management Symposium (SEMI-THERM)*, Santa Clara, CA, 2010, pp. 68–73.
[33] C. Bower, A. Ortega, P. Skandakumaran, R. Vaidyanathan, and T. Phillips, "Heat Transfer in Water-Cooled Silicon Carbide Milli-Channel Heat Sinks for High Power Electronic Applications," *J. Heat Transf.*, vol. 127, no. 1, pp. 59–65, Jan. 2005.
[34] J. A. Carter, L. A. Forster, and M. D. Stitt, "Fabrication and Performance of Tree-Branch Microchannels in Silicon Carbide for Direct Cooling of High-Power Electronics Applications," in *25th Annual IEEE Semiconductor Thermal Measurement and Management Symposium (SEMI-THERM)*, San Jose, CA, 2009, pp. 128–133.
[35] D. B. Tuckerman and R. F. W. Pease, "High-Performance Heat Sinking for VLSI," *IEEE Electron Device Lett.*, vol. 2, no. 5, pp. 126– 129, May 1981.
[36] K. Bennion and G. Moreno, "Thermal Management of Power Semiconductor Packages — Matching Cooling Technologies with Packaging Technologies," presented at the IMAPS 2nd Advanced Technology Workshop on Automotive Microelectronics and Packaging, Dearborn, MI, 2010.
[37] H. Ohtsuka and F. Anraku, "Development of Inverter for 2006 Model Year Civic Hybrid," in *Power Conversion Conference (PCC)*, Nagoya, Japan, 2007, pp. 1596–1600.
[38] F. Anraku, H. Ohtsuka, and T. Masuda, "Compact and High-Power Inverter for 2006 Model Year Civic Hybrid," in *The 22nd International Battery, Hybrid and Fuel Cell Electric Vehicle Symposium & Exposition*, Yokohama, Japan, 2006.
[39] H. Shimizu, T. Okubo, I. Hirano, S. Ishikawa, and M. Abe, "Development of an Integrated Electrified Powertrain for a Newly Developed Electric Vehicle," SAE International, Warrendale, PA, SAE Technical Paper 2013-01-1759, Apr. 2013.
[40] R. J. Moffat, "Modeling Air-Cooled Heat Sinks as Heat Exchangers," in *Twenty Third Annual IEEE Semiconductor Thermal Measurement and Management Symposium (SEMI-THERM)*, San Jose, CA, 2007, pp. 200–207.
[41] K. Bennion and J. Lustbader, "Integrated Three-Dimensional Module Heat Exchanger for Power Electronics Cooling," U.S. Patent 8541875,24-Sep-2013.
[42] R. H. Dieck, *Measurement Uncertainty: Methods and Applications*. ISA, 2007.